

# Ionization rates in a Bose-Einstein condensate of metastable Helium

O. Sirjean, S. Seidelin, J. Viana Gomes, D. Boiron, C. I. Westbrook and A. Aspect  
*Laboratoire Charles Fabry de l'Institut d'Optique, UMR 8501 du CNRS, F-91403 Orsay Cedex, France*

G. V. Shlyapnikov

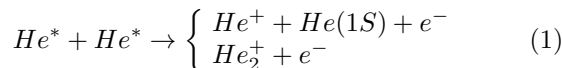
*FOM Institute for Atomic and Molecular Physics, Kruislaan 407, 1098 SJ Amsterdam, The Netherlands*  
*Russian Research Center Kurchatov Institute, Kurchatov Square, 123182 Moscow, Russia*

We have studied ionizing collisions in a BEC of  $\text{He}^*$ . Measurements of the ion production rate combined with measurements of the density and number of atoms for the same sample allow us to estimate both the 2 and 3-body contributions to this rate. A comparison with the decay of the number of condensed atoms in our magnetic trap, in the presence of an rf-shield, indicates that ionizing collisions are largely or wholly responsible for the loss. Quantum depletion makes a substantial correction to the 3-body rate constant.

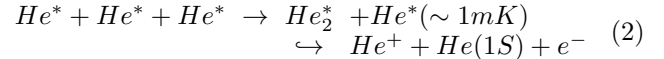
The observation of Bose-Einstein condensation of metastable helium ( $\text{He}$  in the  $2^3S_1$  state, denoted  $\text{He}^*$ ) [1, 2] constituted a pleasant surprise for experimentalists although the possibility had been predicted theoretically [3]. Success hinged, among other things, on a strong suppression of Penning ionization in the spin-polarized, magnetically trapped gas. Too high a rate of ionization would have prevented the accumulation of a density of atoms sufficiently high to achieve evaporative cooling. The ionization rate is not completely suppressed however, and when the atomic density gets high enough, a cold, magnetically trapped sample of  $\text{He}^*$  does produce a detectable flux of ions. As shown in [1], this signal can even be used as a signature of BEC. The observation of ions from the condensate opens the possibility of monitoring in real time the growth kinetics of a condensate [4]. This is an exciting prospect, but in order to quantitatively interpret the ion rate, it is necessary to know the relative contributions of 2 and 3-body collisions.

In this paper we use the unique features of metastable atoms to detect, in a single realization of a BEC, the ionization rate, the density and the number of atoms. This allows us to extract 2 and 3-body rate constants without relying on fits to non-exponential decay of the number of atoms, which require good experimental reproducibility [5, 6, 7] and are notoriously difficult to interpret quantitatively [5]. After estimating the ionization rate constants, a comparison with the observed decay of the number of atoms reveals no evidence for collisional avalanche processes. Thus, by contrast with  $^{87}\text{Rb}$  [8],  $\text{He}^*$  seems to be a good candidate for studying “hydrodynamic” regime as well as the effects of quantum depletion. Indeed in our analysis of the 3-body ionization process, quantum depletion makes a substantial correction [9].

Much theoretical [3, 10] and experimental [1, 2, 11, 12] work has already been devoted to estimating inelastic decay rates in  $\text{He}^*$ . The dominant 2-body decay mechanisms, which we will refer to collectively as Penning ionization,



are known to be suppressed by at least 3 orders of magnitude in a spin-polarized sample, but the total rate constant has not yet been measured. The theoretical estimate of the rate at  $1 \mu\text{K}$  is  $\sim 2 \times 10^{-14} \text{ cm}^3 \text{ s}^{-1}$  [3, 10]. The 3-body reaction,



proceeds via 3-body recombination followed by autoionization of the excited molecule. The rate has been estimated theoretically [13] to have a value of order  $10^{-26} \text{ cm}^6 \text{ s}^{-1}$ . Both reactions yield one positive ion which can easily be detected in our apparatus.

We define collision rate constants according to the density loss in a thermal cloud [14]:  $\frac{dn}{dt} = -\frac{n}{\tau} - \beta n^2 - L n^3$  with  $n$  the local density,  $\tau$  the (vacuum limited) lifetime of the sample, and  $\beta$  and  $L$  the 2-body and 3-body ionizing rate constants defined for a thermal cloud. We have assumed here that there are no other loss processes. One can calculate an expected ionization rate per trapped atom ( $\Gamma$ ):

$$\Gamma = \frac{\text{Ion rate}}{N_0} = \frac{1}{\tau'} + \frac{2}{7} \kappa_2 \beta n_0 + \frac{8}{63} \kappa_3 L n_0^2, \quad (3)$$

for a pure BEC in the Thomas-Fermi regime with a number of atoms  $N_0$ , and a peak density  $n_0$ . The numerical factors come from the integration over the parabolic spatial profile and the fact that although 2 or 3 atoms are lost in each type of collision, only 1 ion is produced. The effective lifetime  $\tau' \geq \tau$  is due to ionizing collisions with the background gas. The factors  $\kappa_i$  take into account the fact that the 2 and 3-particle local correlation functions are smaller than those of a thermal cloud. For a dilute BEC  $\kappa_2 = 1/2!$  and  $\kappa_3 = 1/3!$  [7, 9]. Because the  $\text{He}^*$  scattering length is so large, quantum depletion lead to significant corrections [9] to the  $\kappa$ 's as we discuss below.

Much of our setup has been described previously [1, 15, 16]. Briefly, we trap up to  $2 \times 10^8$  atoms at  $1 \text{ mK}$  in a Ioffe-Pritchard trap with a lifetime ( $\tau$ ) of 90 s. We use a “cloverleaf” configuration [17] with a bias field  $B_0 = 150 \text{ mG}$ . The axial and radial oscillation frequencies in the harmonic trapping potential are  $\nu_{||} = 47 \pm 3 \text{ Hz}$  and

$\nu_{\perp} = 1800 \pm 50$  Hz respectively ( $\bar{\omega}/2\pi = (\nu_{\parallel}\nu_{\perp}^2)^{1/3} = 534$  Hz). A crucial feature of our set up is the detection scheme, based on a 2 stage, single anode microchannel plate detector (MCP) placed below the trapping region. Two grids above the MCP allow us either to repel positive ions and detect only the  $\text{He}^*$  atoms, or to attract and detect positive ions produced in the trapped cloud.

To detect the ion flux, the MCP is used in counting mode: the anode pulses from each ion are amplified, discriminated with a 600 ns deadtime and processed by a counter which records the time delay between successive events. Typical count rates are between  $10^2$  and  $10^4$   $\text{s}^{-1}$ . We have checked that the correlation function of the count rate is flat, indicating that there is no double counting nor any significant time correlation in the ion production. The dark count rate is of order  $1$   $\text{s}^{-1}$ . By changing the sign of the grid voltage, we have checked that while counting ions, the neutral  $\text{He}^*$  detection rate is negligible compared to the ion rate (less than 5 %) even when the radio frequency (rf) shield is on. We estimate the ion detection efficiency by assuming that only ions which hit the open channels of the MCP (60% of the total area) are detected (with a 100% quantum efficiency). We then multiply by the transmission of the two grids  $(0.84)^2$ . Based on Refs. [18, 19], we assume this (0.42) is an upper limit on our detection efficiency.

To find the values of  $N_0$  and  $n_0$  corresponding to the measured ion rate, we use the MCP to observe the time-of-flight signal (TOF) of the  $\text{He}^*$  atoms released from the rapidly switched off trap. The instantaneous count rate can be as high as  $10^6$   $\text{s}^{-1}$ , and the MCP saturates when used in counting mode. To avoid this problem, we lower the MCP gain, and record the TOF signal in analog mode with a time constant of 400 microseconds. Several tests were performed to verify the linearity of the detector.

In a typical run, forced evaporative cooling takes place for 40 s, down to an rf-knife frequency of 500 KHz, about 50 kHz above the minimum of the trapping potential. Near the end of the ramp, the ion rate increases sharply, signaling the appearance of a BEC (Fig. 4 in [1]). After reaching the final value, the rf-knife is held on at that frequency (rf-shield). The above sequence results in a quasi pure BEC for delay times up to 15 s (see Fig. 3). By quasi-pure we mean that we see no evidence of any thermal wings in signals such as shown in the inset of Fig. 1. From tests of our fitting procedure, we estimate that the smallest thermal fraction we can distinguish is about 20 %, corresponding to a temperature on the order of the chemical potential. Runs in which thermal wings were visible were discarded.

To acquire the TOF signals corresponding to a given ion rate, we turn off the rf-shield, wait 50 ms, and then turn off the magnetic trap, and switch the MCP to analog mode. To be sure that the rf has no influence on the ion rate, we use only the number of ions observed during the 50 ms delay to get the rate. We fit the TOF signals to an inverted parabola squared as expected for a pure BEC in the Thomas-Fermi regime, and for a TOF width ( $\sim 5$  ms)

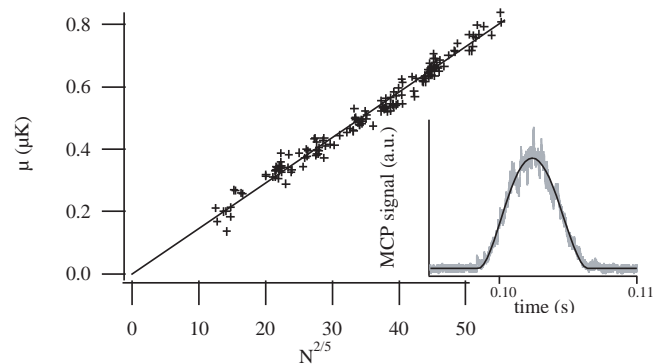


FIG. 1: Chemical potential versus number of detected atoms to the power  $\frac{2}{5}$  and its linear fit. Data are for quasi-pure BEC. Inset shows a typical TOF signal and its inverted parabola squared fit.

narrow compared to the mean arrival time (100 ms) [1]. Under these assumptions, the chemical potential  $\mu$  depends only on the TOF width, the atomic mass and the acceleration of gravity [20], and thus can be measured quite accurately. Figure 1 shows that  $\mu$  varies as  $N_0^{2/5}$  as expected, over almost 2 decades in atom number. Residuals from the linear fit do not show any systematic variation which is a good indication of the detection linearity. A fit on a log-log plot gives a slope of 0.39.

To determine the collision rate constants  $\beta$  and  $L$ , we need an absolute calibration of the number of atoms and the density. As discussed in Ref. [1], all the atoms are not detected, and the direct calibration has a 50 % uncertainty which is responsible for the large uncertainty in the scattering length  $a$ . In fact the measurement of the chemical potential gives an accurate value for the product  $n_0 a = \mu m / 4\pi \hbar^2$ , and with the value of  $\bar{\omega}$  gives the product  $N_0 a = (1/15) (\hbar/m\bar{\omega})^{1/2} (2\mu/\hbar\bar{\omega})^{5/2}$  as well. Therefore, in the hopes that the  $\text{He}^*$  scattering length will be measured more accurately in the future, we shall express  $N_0$  and  $n_0$  in terms of  $a$ . In this paper, unless stated otherwise, we suppose that  $a = 20$  nm, and in our conclusions we shall discuss how our results depend on  $a$ .

Figure 2 shows the ion rate per atom  $\Gamma$  versus the peak density. The densest sample corresponds to  $N_0 = 2 \times 10^5$  atoms and  $n_0 = 2.5 \times 10^{13}$   $\text{cm}^{-3}$ . The corresponding Thomas-Fermi radii are  $r_{\perp} \simeq 5$   $\mu\text{m}$  and  $r_{\parallel} \simeq 200$   $\mu\text{m}$ . The vertical intercept in Fig. 2 corresponds to ionizing collisions with the background gas ( $1/\tau'$ ). We have independently estimated this rate using trapped thermal clouds at 1 mK and 5  $\mu\text{K}$ , and found  $1/\tau' \lesssim 5 \times 10^{-3}$   $\text{s}^{-1}$ . This value is negligible at the scale of the figure.

The curvature seen in Fig. 2 shows that 3-body ionizing collisions are significant. Before fitting the data to get  $\beta$  and  $L$ , we must take into account several effects. First, for 3-body collisions, quantum depletion is important. For  $T = 0$ , reference [9] gives a multiplicative correction [21] to the factor  $\kappa_3$  of  $((1 + \epsilon) = (1 + A \frac{73}{\sqrt{\pi}} \times \sqrt{n_0 a^3}))$ ,

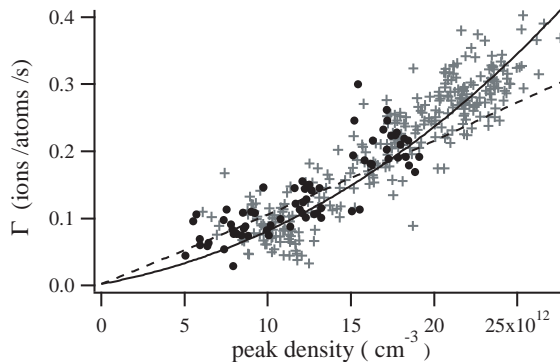


FIG. 2: Ion rate per trapped atom versus peak density for 350 different quasi-pure BEC's. Atom number and density are deduced from  $\mu$ ,  $\bar{\omega}$  and  $a$  (here 20 nm). Data were taken for 2 different bias fields corresponding to  $\nu_{\perp} = 1800$  Hz (crosses) and  $\nu_{\perp} = 1200$  Hz (circles). The dashed line corresponds to the best fit involving only 2-body collisions. The solid line is a fit to 2 and 3-body processes.

where  $A \simeq 0.84$  and comes from an integration over the spatial profile using a local density approximation. At our highest density  $\epsilon \simeq 0.5$ . Two-body collisions are subject to an analogous correction but approximately 3 times smaller. The fits in Fig. 2 include the density dependence of  $\kappa_{2,3}$ , associated with quantum depletion. The  $n_0^{3/2}$  dependence introduced for 2-body collisions is far too small to explain the curvature in the data. The density dependence of  $\kappa_{2,3}$  does not significantly improve the quality of the fit, but it significantly affects the value of the fitted value of  $L$  (reduction of 40%).

In addition, the fact that the sample probably contains a small thermal component means that collisions between the condensed and the thermal parts must be taken into account [6, 9]. Assuming a 10 % thermal population ( $\frac{\mu}{k_B T} \simeq 1.1$ ), we find  $\kappa_3 = \frac{1}{6}(1 + \epsilon + \epsilon')$ , with an additional correction  $\epsilon' \simeq 0.35$  for the densest sample [22].

Taking into account all these corrections, the fitted values of the collision rate constants [14] are:  $\beta_{20} = 2.9(\pm 2.0) \times 10^{-14} \text{ cm}^3 \text{ sec}^{-1}$  and  $L_{20} = 8.5(\pm 5.3) \times 10^{-27} \text{ cm}^6 \text{ sec}^{-1}$ , where the subscripts refer to the assumed value of  $a$ . These values are in good agreement with the theoretical estimates. The error bars are estimated as follows. We fix either  $\beta$  or  $L$  and use the other as a fit parameter. We repeat this procedure for different values of the fixed parameter and take the range over which we can get a converging and physically reasonable fit (i.e. no negative rate constants) as the uncertainty in the fixed parameter. These error bars are highly correlated since if  $\beta$  is increased,  $L$  must be decreased and vice-versa. The error bars do not include the uncertainty in the absolute ion detection efficiency (see below).

Until now we have assumed  $a = 20$  nm, but current experiments give a range from 8 nm to 30 nm [1, 2]. Using Eq. 3 and our parameterization of  $n_0$  and  $N_0$  in terms

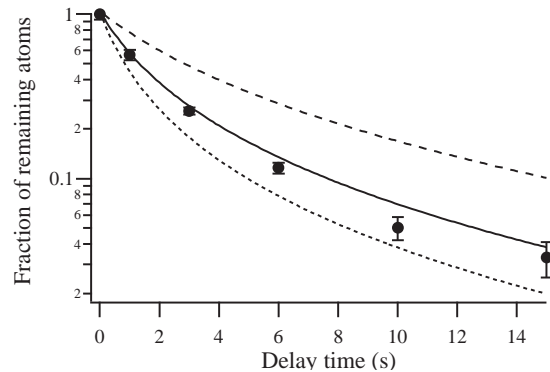


FIG. 3: Fraction of remaining atoms measured by TOF as a function of time. The rf-shield is on and the cloud remains a quasi pure condensate during the decay. The lines correspond to the predicted atom decay according to Eq. 3 with the fitted value of the 2- and 3-body rate constants for  $a = 10$  nm (dashed line),  $a = 20$  nm (solid line) and  $a = 30$  nm (dotted line). The case of  $a = 10$  nm is not necessarily excluded because other, non-ionizing losses could be present.

of  $a$ , one can see that, in the absence of quantum depletion, the values of  $\beta$  and  $L$  extracted from our analysis would be proportional to  $a^2$  and  $a^3$  respectively. Taking quantum depletion into account, no simple analytical dependence exists, but one can numerically evaluate  $\beta$  and  $L$  vs.  $a$  and fit the results to expansions with leading terms in  $a^2$  and  $a^3$  respectively. The effect of quantum depletion is negligible for  $\beta$  ( $\beta_a \approx \beta_{20}(\frac{a}{20})^2$ ). For  $L$ , we find  $L_a \approx L_{20}(\frac{a}{20})^3[1 - 0.23\frac{a-20}{20}]$  with  $a$  in nm.

To test the consistency of our measurements, we have studied the decay of the number of atoms in the BEC (Fig. 3). To acquire these data, we held the BEC in the trap in the presence of the rf-shield for varying times. This study involves multiple realizations of a BEC, which typically exhibit large fluctuations in the initial atom number. We have been able to reduce this noise by using the ion signal to select only data corresponding to the same ion rate 500 ms after the end of the ramp. This time corresponds to  $t = 0$  in the figure. We have also plotted the predicted decay curve (solid line) corresponding to ionization only. This curve results from a numerical integration of the atom loss due to ionization processes, calculated from the fitted values  $\beta_{20}$  and  $L_{20}$ . The fact that the error bars on  $\beta$  and  $L$  are correlated leads to a small uncertainty on the solid curve that happens to be of the same order of magnitude as the typical error bars on the data. The observed decay agrees fairly well with the solid curve, and ionization apparently accounts for most of the loss. If the ion detection efficiency were actually lower than we assume, the predicted decay due to ionization would be faster than the observed decay, an unphysical situation. From this, we conclude that our estimate of the detection efficiency is accurate and does not lead to an additional uncertainty in  $\beta$  and  $L$ .

We have also plotted the curves obtained from the same analysis but with scattering lengths of 10 and 30 nm. The curve corresponding  $a = 30$  nm lies below the data points. Based on our analysis, this means that  $a = 30$  nm is excluded. A scattering length of  $a = 25$  nm is the largest one consistent with our data. In contrast, the decay predicted for an analysis with  $a = 10$  nm is slower than the observed decay of the number of condensed atoms. This would mean that there are additional non-ionizing losses (contributing up to half of the total loss), and/or that we have overestimated the ion detection efficiency by a factor as large as 2. In the latter case, the rate constants  $\beta$  and  $L$  should be multiplied by the same factor. This results for  $a = 10$  nm in a supplementary systematic uncertainty on  $\beta$  and  $L$  of a factor as large as 2.

Even though the peak densities of our BEC are small compared to those in alkalis, the elastic collision rate is high because of the large scattering length, and one must consider the possibility of collisional avalanches. For  $a = 20$  nm our densest cloud has a mean free path of  $(8\pi a^2 \bar{n})^{-1} \approx 7\mu\text{m}$  and using the definition of [8] the collisional opacity is  $\approx 0.8$ . With Rb atoms this would result in avalanche processes increasing by a large amount the atom loss [8]. In our case we have to consider secondary collisions leading to both ion production and atom loss. However, no product of an ionizing collision can produce many secondary ionizing collisions, since the corresponding mean free paths are at least two orders of

magnitude larger than  $r_{\parallel}$ . Hence secondary ionization is unimportant and Eq. 3 correctly describes the ionizing processes. This conclusion is supported by our observation that no correlation exists in the time distribution of detected ions.

The good agreement between the data and the curve in Fig. 3 indicates that losses due to non-ionizing collisional avalanches are not taking place either. This is in agreement with data on elastic collisions with  $\text{He}^+$ ,  $\text{He}_2^+$  and  $\text{He}(1S)$ , which have small cross sections [23]. Collisions with hot  $\text{He}^*$  atoms from the reaction of Eq. 2 are more likely to play a role, but due to the higher velocity, the elastic cross section for these atoms is smaller. This is in contrast to what happens with Rb atoms [8] where the total cross section is enhanced due to d-wave scattering resonance.

The theoretical analysis shows that quantum depletion strongly affects the measured 3-body rate constant. One way to experimentally demonstrate this effect would be to do similar measurements with thermal clouds, and compare them with the results reported here. Absolute calibration of ion and atom detection efficiency should play no role in this comparison, if one could prove that they are the same for both situations.

We thank F. Gerbier for stimulating discussions. Supported by the European Union under grants IST-1999-11055 and HPRN-CT-2000-00125, and by the DGA grant 00.34.025.

- 
- [1] A. Robert *et al.*, Science **292**, 461 (2001).  
 [2] F. Pereira Dos Santos *et al.*, Phys. Rev. Lett. **86**, 3459 (2001).  
 [3] G. V. Shlyapnikov *et al.*, Phys. Rev. Lett. **73**, 3247 (1994); P. O. Fedichev *et al.*, Phys. Rev. A **53**, 1447 (1996).  
 [4] H. J. Miesner *et al.*, Science, **270**, 1005 (1998); M. Köhl *et al.*, Phys. Rev. Lett. **88**, 080402 (2002).  
 [5] J. L. Roberts *et al.*, Phys. Rev. Lett. **85**, 728 (2000).  
 [6] J. Söding *et al.*, Appl. Phys. B **69**, 257 (1999).  
 [7] E. A. Burt *et al.*, Phys. Rev. Lett. **79**, 337 (1997).  
 [8] J. Schuster *et al.*, Phys. Rev. Lett. **87**, 170404 (2001).  
 [9] Y. Kagan, B. V. Svistunov, and G. V. Shlyapnikov, JETP Lett. **42**, 209 (1985).  
 [10] V. Venturi *et al.*, Phys. Rev. A **60**, 4635 (1999); V. Venturi and I. B. Whittingham, Phys. Rev. A **61**, 060703(R) (2000).  
 [11] J. C. Hill *et al.*, Phys. Rev. A **5**, 189 (1972).  
 [12] N. Herschbach *et al.*, Phys. Rev. A **61**, 50702 (2000).  
 [13] P. O. Fedichev, M. W. Reynolds, and G. V. Shlyapnikov, Phys. Rev. Lett. **77**, 2921 (1996); P. F. Bedaque, E. Braaten, and H. W. Hammer, Phys. Rev. Lett. **85**, 908 (2000).  
 [14] Collision rate constants are sometimes defined directly for a BEC ( $\beta' = \beta/2$  and  $L' = L/6$ ).  
 [15] A. Browaeys *et al.*, Phys. Rev. A **64**, 034703 (2001).  
 [16] S. Nowak *et al.*, Appl. Phys. B **70**, 455 (2000).  
 [17] M. O. Mewes *et al.*, Phys. Rev. Lett. **77**, 416 (1996).  
 [18] B. Deconihout *et al.*, Appl. Surf. Sci. **94/95**, 422 (1996).  
 [19] R. S. Gao *et al.*, Rev. Sci. Instrum. **55**, 1756 (1984).  
 [20] Y. Castin and R. Dum, Phys. Rev. Lett. **77**, 5315 (1996); Y. Kagan, E.L. Surkov, and G. V. Shlyapnikov, Phys. Rev. A **54**, 1753 (1996).  
 [21] The numerical factor 64 of [9] is replaced by a factor 72 because here we express the decay rate in terms of the condensate density  $n_0$ , not in terms of the total density.  
 [22] For  $T \sim \mu$ , we have  $\epsilon' \approx < 3/\pi^2 \int_0^\infty (\frac{3E_k}{2\epsilon_k(r)} + \frac{\tilde{\mu}(r)}{2\epsilon_k(r)}) \frac{1}{e^{\epsilon_k(r)/k_b T} - 1} k^2 dk / n(r) >$  with  $n(r)$  the local density of the BEC,  $E_k = \frac{\hbar^2 k^2}{2m}$ ,  $\epsilon_k(r) = \sqrt{E_k^2 + 2\tilde{\mu}(r)E_k}$ , and  $\tilde{\mu}(r)$  the local chemical potential. The brackets indicate spatial averaging. This can be written :  $48 \sqrt{\frac{2}{\pi}} \times \sqrt{n_0 a^3} \times A'(\frac{\mu}{k_b T})$ . The numerical factor  $A'$  comes from the integration over the spatial profile and takes implicitly into account the overlap of the BEC with the thermal cloud. We find  $A'(\frac{\mu}{k_b T} = 1.1) \simeq 0.65$ .  
 [23] H. C. W. Beijerinck *et al.*, Phys. Rev. A **61**, 23607 (2000).